

Article

Phenotyping the Anthocyanin Content of Various Organs in Purple Corn Using a Digital Camera

Zhengxin Wang^{1,†}, Ye Liu^{2,†}, Ke Wang¹, Yusong Wang¹, Xue Wang¹, Jiaming Liu¹, Cheng Xu³
and Youhong Song^{1,4,*} 

¹ School of Agronomy, Anhui Agricultural University, Hefei 230036, China; zwxwang@ahau.edu.cn (Z.W.); 22721735@stu.ahau.edu.cn (K.W.); wangyusong03@stu.ahau.edu.cn (Y.W.); xuawang@stu.ahau.edu.cn (X.W.); ljming@stu.ahau.edu.cn (J.L.)

² Department of Geographical and Earth Sciences, University of Glasgow, Gilmorehill, Glasgow G12 8QQ, UK; liuye5361@163.com

³ School of Economics and Management, Jingdezhen University, Jingdezhen 333400, China; jgzxc_2005@163.com

⁴ Centre for Crop Science, Queensland Alliance for Agriculture and Food Innovation, The University of Queensland, Brisbane, QLD 4072, Australia

* Correspondence: uqysong@163.com

† These authors contributed equally to this work.

Abstract: Anthocyanins are precious industrial raw materials. Purple corn is rich in anthocyanins, with large variation in their content between organs. It is imperative to find a rapid and non-destructive method to determine the anthocyanin content in purple corn. To this end, a field experiment with ten purple corn hybrids was conducted, collecting plant images using a digital camera and determining the anthocyanin content of different organ types. The average values of red (R), green (G) and blue (B) in the images were extracted. The color indices derived from RGB arithmetic operations were applied in establishing a model for estimation of the anthocyanin content. The results showed that the specific color index varied with the organ type in purple corn, i.e., AC_{CR} for the grains, BRT for the cobs, AC_{CB} for the husks, R for the stems, AC_{CB} for the sheaths and BRT for the laminae, respectively. Linear models of the relationship between the color indices and anthocyanin content for different organs were established with R^2 falling in the range of 0.64–0.94. The predictive accuracy of the linear models, assessed according to the NRMSE, was validated using a sample size of 2:1. The average NRMSE value was 11.68% in the grains, 13.66% in the cobs, 8.90% in the husks, 27.20% in the stems, 7.90% in the sheaths and 15.83% in the laminae, respectively, all less than 30%, indicating that the accuracy and stability of the model was trustworthy and reliable. In conclusion, this study provided a new method for rapid, non-destructive prediction of anthocyanin-rich organs in purple corn.

Keywords: purple corn; anthocyanin; digital photography; image analysis



Citation: Wang, Z.; Liu, Y.; Wang, K.; Wang, Y.; Wang, X.; Liu, J.; Xu, C.; Song, Y. Phenotyping the Anthocyanin Content of Various Organs in Purple Corn Using a Digital Camera. *Agriculture* **2024**, *14*, 744. <https://doi.org/10.3390/agriculture14050744>

Academic Editor: Marcus Randall

Received: 15 March 2024

Revised: 5 May 2024

Accepted: 7 May 2024

Published: 10 May 2024



Copyright: © 2024 by the authors. Licensee MDPI, Basel, Switzerland. This article is an open access article distributed under the terms and conditions of the Creative Commons Attribution (CC BY) license (<https://creativecommons.org/licenses/by/4.0/>).

1. Introduction

Anthocyanins are natural pigments with a wide range of colors and represent a major subclass of polyphenols/flavonoids [1]. Such pigments are widely found in natural plants, playing a critical role in alleviating the effect of biotic and abiotic stresses [2–6]. They are also used widely in the food, pharmaceutical and cosmetics industries due to their natural, non-toxic and antioxidant properties [7–10]. As reported, the global market of flavonoids is valued at USD 1.06 billion by 2025, and anthocyanins account for the majority of this share [11]. In the foreseeable future, the demand for anthocyanins in industry will continue to grow [12,13].

The most common way to obtain anthocyanins is to extract them from different plant sources, such as fruits and flowers, but the economic benefit of this is low since such

materials are costly [14–16]. Extracting anthocyanins from agricultural by-products such as fruit crops is considered to be a cost-effective method [17,18]. Among them, purple corn (*Zea mays* L.) has attracted significant attention due to the abundance of anthocyanins in its non-grain tissues, such as the cob, in addition to the grain [19,20]. Nevertheless, the procedure of measuring anthocyanin content is cumbersome, as it involves isolating and grinding plant tissues, then the chemical extraction of anthocyanins and analysis of absorbance values or chromatography [14]. It is fairly tedious and costly if many samples are considered in practice [21]. Hence, it is essential to find a simple, convenient method for rapidly estimating the anthocyanin content in different organs in purple corn.

Digital images acquired using sensors such as RGB, multispectral, hyperspectral, thermal infrared and LiDAR have been widely used in monitoring plant height, leaf area indices and plant nutrients [22,23]; the detection of pests and disease [24,25] and the prediction of crop yield [26]. Recently, studies have shown that the color parameters of digital images acquired using RGB cameras can be used to predict the pigment content in plant tissues, such as their content of chlorophyll and anthocyanins [27–29]. In addition, a chlorophyll quantification system based on images from digital cameras such as smartphone and digital single-lens cameras was developed to accurately quantify the chlorophyll content of *Chlamydomonas*, quinoa and amaranth leaves in situ [30,31]. It has been reported that the color indices of RGB channel values are significantly correlated with the pigment content, indicating that modeling based on such relations is feasible [32–34].

To our knowledge, the anthocyanin content in plant tissues has been estimated using digital images only in black rice [35], sugar maple [36] and some flowers from Spain, including *Borago officinalis* L., *Malva sylvestris* L., *Orchis italica* Poir. and *Silene littorea* Brot [28]. Thus far, there has been no report on purple corn plants. Within this context, we carried out a field study with 10 purple corn hybrids to phenotype the anthocyanin content of various types of organs. Thus, the aim of this study was to (i) examine the relationship between the anthocyanin content in different organs and the color indices of visible light images; (ii) determine the optimal color index for modeling different organs of purple corn and (iii) evaluate the stability of the established predictive model.

2. Materials and Methods

2.1. Plant Materials and Sampling

Ten hybrids of purple corn were sown on 12 June 2022 at the experimental station of Anhui Agricultural University, Hefei (31°86' N, 117°25' E, altitude = 27.05 m), Anhui Province, China. We carried out a comparison with the findings in Wang et al. (2022) on meteorological data from different locations in Huaibei Plain, Anhui Province, for 61 years [37]. Among them, the range of \bar{T}_{\max} is 29.97–32.94 °C, while the range of \bar{T}_{\min} is 20.99–25.08 °C, and the range of \bar{T}_{mean} is 25.04–28.59 °C. Our data are consistent with the historical law of this region with similar climate attributes (see Figure S1 and Table S1). Therefore, it can be considered a typical year.

The soil at the experimental field was a yellow brown type with medium fertility. The planting density was 52,500 plants·ha⁻¹, with 60 cm spacing between rows. A random complete block design was adopted with 3 replicates for each variety. Fertilizer was applied with a mixture of urea, calcium superphosphate and potassium sulfate, adding up to 60.0 kg·ha⁻¹ of P₂O₅, 75.0 kg·ha⁻¹ of K₂O, 187.5 kg·ha⁻¹ of pure nitrogen and one-third nitrogen fertilizer as the base fertilizer, and the rest of the nitrogen fertilizer was applied at the big-flare stage. Field management was carried out by following conventional field cultivation techniques. Because previous studies found that anthocyanins are the main cause of plant coloration [38,39], in order to obtain the maximum range of color variation, we focused on the anthocyanin-rich organs of purple corn (Table 1). In this paper, purple corn plants of different hybrids at vegetative stages (V12–VT) and reproductive stages (R1–R4) in the experimental field were retrieved, and the organs rich in anthocyanins were decomposed, photographed and numbered.

Table 1. Information on various organs containing anthocyanins in 10 hybrids.

Variety	Organ with Anthocyanins	Growth Period
SGHN	Grain, Cob, Husk, Stem, Sheath, Lamina	85 days
ZZN8	Grain, Cob, Husk, Stem, Sheath, Lamina	85 days
JHN3	Grain, Cob, Husk	85 days
HTN168	Grain, Cob, Husk	85 days
SD31	Grain, Cob, Husk	86 days
HTN520	Grain	80–85 days
TNBM508	Grain	85 days
TNHB509	Grain	85 days
JZXN	Grain	80–85 days
HZHN1	Grain	90 days

2.2. Digital Image Acquisition and Preprocessing

The procedure for acquiring and standardizing the digital images is shown in Figure 1. First, we used a Canon EOS M50 Mark II camera (Canon Corporation, Tokyo, Japan) equipped with an EF-M 14–45 mm autofocus lens (transmitting wavelengths of 370–700 nm). This camera has a 22.3×14.9 mm CMOS sensor (6000×4000 pixels) and shows full regulation of exposure and metering, as recommended for unbiased data acquisition [40]. We manually adjusted these settings for all the samples: a shutter speed of $1/40$, a lens aperture of $f/3.5$, ISO 100, and white balance fixed at 4500 k. The photos were underexposed by +1.7 to prevent color “clipping” or saturation, and we used a uniform illuminance of 500 lx light for illumination [41]. The images were taken in canon RAW format (CR3) because RAW files of unprocessed images can be linearized using specialized software. For the acquisition of images of each organ of the purple corn plants, each sample in this study was photographed using a Calibrite ColorChecker Classic standard 24-color card (X-Rite Inc., Grand Rapids, MI, USA). Due to the significant effect of different lighting on RGB channel color parameters, the light conditions were standardized for different shooting environments [42,43]. First, a profile was created with conversion from RAW into DNG format using ColorChecker Camera Calibration (X-Rite Inc., Grand Rapids, MI, USA). Second, the constructed profile was selected for color calibration using Adobe Lightroom Classic software (v11.5, Adobe, Inc., San Jose, CA, USA). Finally, the non-experimental areas of the digital images were segmented and removed using Adobe Photoshop 2020 software (v23.5, Adobe, Inc., San Jose, CA, USA) to eliminate their influence on the extraction of the color parameters. After this series of image processing processes, color-calibrated images were obtained [44].

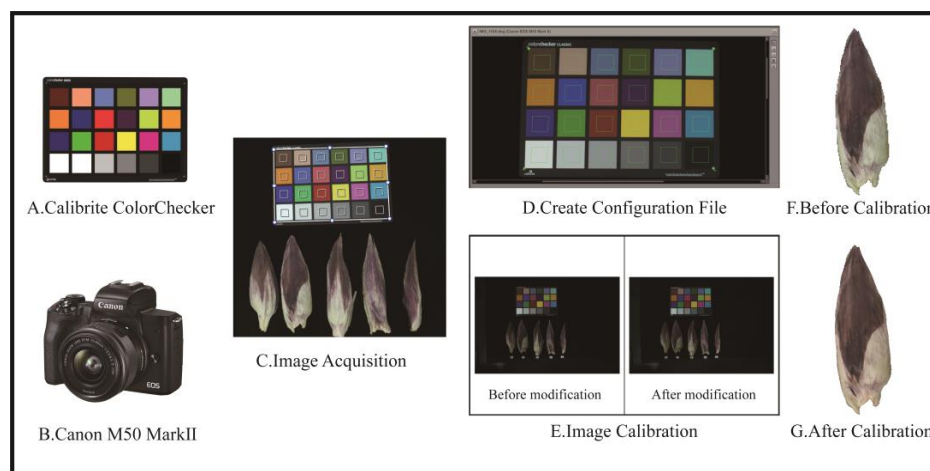


Figure 1. Digital image acquisition and standardization process. (A) A picture of the X-Rite ColorChecker classic chart. (B) The camera used in the experiment. (C) The sample image acquisition. (D) Creation of DNG format file in Colorchecker Camera Calibration. (E) Image calibration in Lightroom. (F) The image before color calibration. (G) The image after color calibration.

2.3. Image Analysis and Processing of the Color Data

RGB color channels are a natural color mode that can represent 16 million colors in nature. Numerous color feature indices can be obtained using these channels. However, by referring to the selection of color indices in similar studies, in this study, in addition to the R, G and B parameters in the RGB channels, 11 indices commonly used in previous studies on the relationship between pigment content and RGB were selected as alternatives, and their calculation methods and the related literature are shown in Table 2.

Table 2. Color indices used to estimate anthocyanin content from digital image data.

Color Indices	Formula Used for Digital Images	References
Red:green ratio	$RG_R = N_{red}/N_{green}$	[45]
Red:blue ratio	$RB_R = N_{red}/N_{blue}$	[45]
Green:blue ratio	$GB_R = N_{green}/N_{blue}$	[45]
Strength of red	$S_{red} = N_{green}/(N_{red} + N_{green} + N_{blue})$	[46]
Strength of green	$S_{green} = N_{green}/(N_{red} + N_{green} + N_{blue})$	[46]
Strength of blue	$S_{blue} = N_{green}/(N_{red} + N_{green} + N_{blue})$	[46]
Brightness	$BRT = \sqrt{[(S_{blue}^2 + S_{green}^2 + S_{red}^2)/3]}$	[28]
Chroma	$C = (N_{red} - N_{green})/[(N_{red} + N_{green} + N_{blue})/3]$	[28]
Anthocyanin content, chroma basic	$AC_{CB} = (N_{blue} + N_{red})/N_{green}$	[28]
Anthocyanin content, chroma ratio	$AC_{CR} = N_{green}/[(N_{blue} + N_{red})/2]$	[28]
Anthocyanin content, chroma difference	$AC_{CD} = (N_{blue} + N_{red})/2 - N_{green}$	[28]

2.4. Extraction and Quantification of Anthocyanin

To determine the anthocyanins in the different organs of purple corn, the solvent extraction method mentioned by Tan and Bai et al. [47,48] was adopted and improved. The extraction agent was a mixture of ethanol and hydrochloric acid (95% ethanol and 1.5 mol/L hydrochloric acid, volume ratio of 85:15). The sample was placed in a 10 mL centrifuge tube, heated in a water bath at 80 °C for 30 min and centrifuged at 10,000 r·min⁻¹ for 10 min. Then, the supernatant was taken, and this was repeated three times after combining the extraction solution volume to 25 mL. After cooling, the OD value of the extracted solution at 535 nm was determined using an ultraviolet spectrophotometer.

2.5. Establishment and Validation of the Model

Because our primary goal was to test whether the anthocyanin content could be predicted from the values of the indices obtained from the digital images, we used least squares linear regression to test this [49]. Preliminary graphic inspection showed that our data were appropriate for a simple regression model [50]. As for the establishment of a model of the anthocyanin content, this study adopted the isometric sampling method to screen the modeling samples and the validation samples, conducting the isometric sampling with a modeling:validation ratio = 2:1, and compared the coefficient of determination (R²) of the fitting equation and the root mean square error (RMSE) to determine the optimal image color indices and establish a prediction model. For validation of the prediction model, we used the RMSE and the normalized root mean square error (NRMSE) for the evaluation [51]. In general, an R² value higher than 0.7 is considered indicative of a good model that can explain a significant amount of variance, while a higher value indicates a better model fit. A lower RMSE value indicates a better model fit because it measures the deviation between the predicted value and the observed value and is sensitive to outliers in the data [52,53]. The simulation is considered excellent with an NRMSE ≤ 10%, good if it is 10–20%, fair if it is 20–30% and poor if it is >30% [54].

$$RMSE = \sqrt{\frac{1}{n} \times \sum_{i=1}^n (SIM_i - OBS_i)^2}$$

$$\text{NRMSE} = \sqrt{\frac{1}{n} \times \sum_{i=1}^n (\text{SIM}_i - \text{OBS}_i)^2} \times \frac{1}{\overline{\text{OBS}}} \times 100\%$$

where SIM_i and OBS_i represent the simulated and observed values, respectively, $\overline{\text{OBS}}$ represents the observed mean value and n is the number of samples.

2.6. Statistical Analysis

Analysis of variance (ANOVA) was performed using SPSS software (v19.0, SPSS, Inc., Chicago, IL, USA). The means were compared using Tukey's LSD (least significant difference) test at $p < 0.05$. Microsoft Excel software (v2021, Microsoft, Inc., Redmond, WA, USA) was used to sort out the test data and produce graphs and tables. Origin 2019 software (v10.1.0.40, OriginLab, Inc., Northampton, MA, USA) and Adobe Illustrator software (v26.5.0, Adobe, Inc., San Jose, CA, USA) were used for drawing.

3. Results

3.1. Anthocyanin Content of Various Organs in Purple Corn

The anthocyanin content of the specific types of organs across various hybrids is shown in Table 3. There were significant differences ($p < 0.05$) in the grain anthocyanin content among different hybrids, of which the highest anthocyanin content was 33.26 mg/100 g in HTN520, while the lowest anthocyanin content was 7.11 mg/100 g in JZXN. Notably, the anthocyanin content in HTN520 is 4.7 times greater than that in JZXN. This difference is caused by hybrid genotypes, and breeding varieties rich in functional phytochemicals such as anthocyanins is considered necessary and will be beneficial to the health of consumers [55,56]. Further analyses uncovered differences in the anthocyanin contents of the other organs. The anthocyanin content of the cob part ranged from 143.84 mg/100 g to 1334.10 mg/100 g. It is worth noting that the anthocyanin content in the cob was 188 times higher than that in the grain. Similarly in the husk part, the anthocyanin content ranged from 91.27 to 862.33 mg/100 g, which was slightly lower than that of the cob part but also significantly higher than that of the grain part, by up to 121 times. In SGHN and ZZN8, there were significant differences in the content of anthocyanins in the sheath parts, and the anthocyanin content of the sheaths was also significantly higher than that of the grain parts, but no significant differences were found for the sheath and lamina parts.

Table 3. Anthocyanin content of different organs in ten purple corn varieties.

Variety	Anthocyanin Content of Specific Organ Type (mg/100 g)					
	Grain	Cob	Husk	Sheath	Lamina	Stem
SGHN	22.22 de	1183.12 d	862.33 a	201.23 a	37.40 a	17.02 a
ZZN8	24.39 cd	1334.10 a	650.48 b	126.10 b	39.45 a	12.25 a
JHN3	27.65 bc	292.74 c	336.46 c			
HTN168	30.84 ab	295.22 c	205.73 d			
SD31	19.94 ef	143.84 d	91.27 e			
HTN520	33.26 a					
TNBM508	16.24 f					
TNHB509	7.29 g					
JZXN	7.11 g					
HZHN1	20.60 de					

Note: Different lowercase letters within a column indicate significant differences ($p < 0.05$) in anthocyanin content between different organs.

At present, the recovery of bioactive compounds from food by-products to obtain higher returns has been widely studied [19,20,57]. According to the above analysis, the cobs, husks and sheaths of purple corn contain a large amount of anthocyanin resources, which can be used as good raw material for the industrial extraction of anthocyanins and should be paid attention to in industrial production.

3.2. Correlation Analysis of Anthocyanin Content and Color Indices in Purple Corn

A heat map of the correlation between the anthocyanin content and common color indices is shown in Figure 2. In the visible light band, the anthocyanin content of specific organ types in purple corn is mostly negatively correlated with their R, G and B values; in particular, the transformed RG_R , RB_R , GB_R , C, BRT, AC_{CB} and AC_{CR} values had a highly significant correlation ($p < 0.01$). This is consistent with previous research results. In general, the darker the color of plant tissue (the lower the RGB value), the higher the pigment content [28,58,59]. In addition, of the 14 color indices, the color index most highly correlation with the anthocyanin content varied according to the organ type. For example, AC_{CR} and RBR were determined for the grain, BRT and R for the cob, AC_{CB} and AC_{CD} for the husk, R for the stem, AC_{CB} for the sheath and BRT for the lamina.

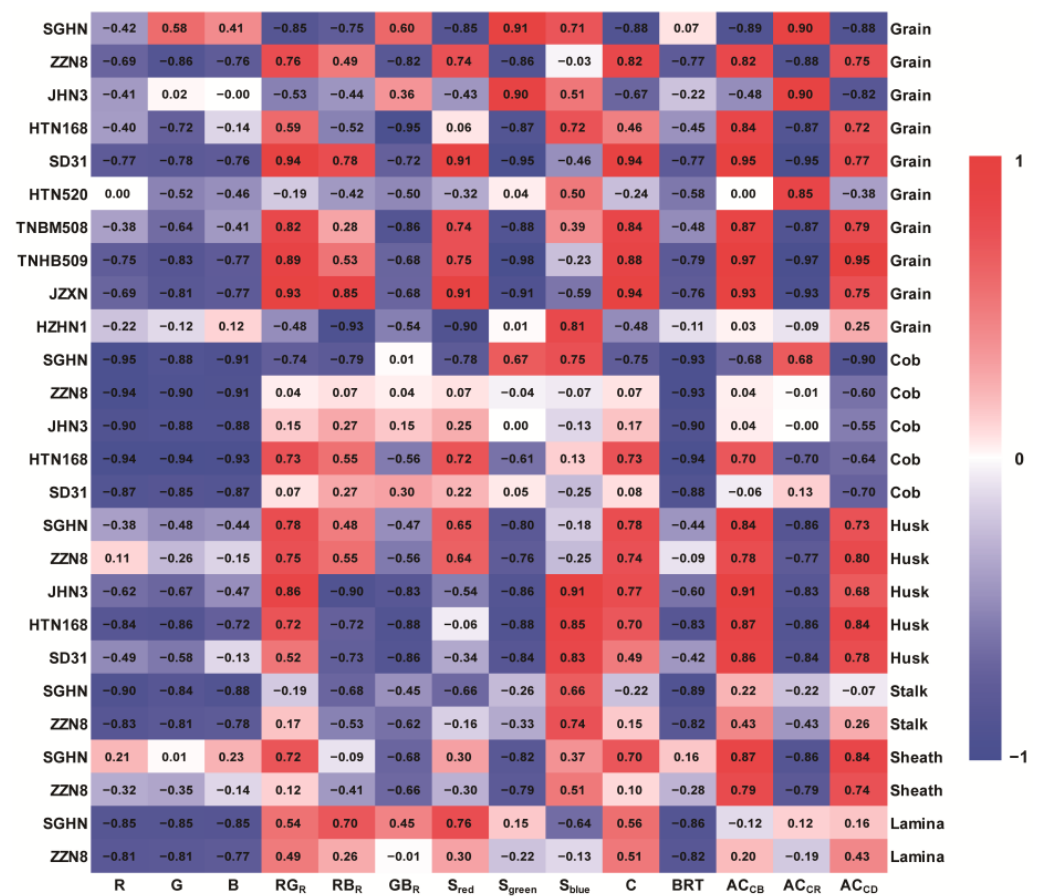


Figure 2. Visual heat map of the correlation between anthocyanin content and color indices in different organs.

3.3. Fitting Robustness of the Relationships between Anthocyanin Content and the Color Indices

Modeling samples were used for linear fitting based on 14 color indices, respectively, and the regression results are shown in Table 4. The color indices with the best goodness of fit were as follows: AC_{CB} (eight studied samples), AC_{CR} (seven studied samples), BRT (five studied samples), R (four studied samples), RB_R (one studied sample) and AC_{CD} (one studied sample). This suggests that such indices can be used in indicating the anthocyanin content. The optimal predictive model for anthocyanin content is shown in Figure 3. The coefficient of determination (R^2) for the fittings on the grain anthocyanin content (Figure 3A) ranged from 0.71 to 0.94. The R^2 of the predictive model for the cob anthocyanin content (Figure 3B) ranged from 0.80 to 0.87. The model error for the grains was smaller than that for the cobs, and the fitting effect for both parts was very good ($R^2 > 0.70$). For the husks (Figure 3C) and sheaths (Figure 3D), with heterogeneous pigmentation patterns, the R^2

ranged from 0.70 to 0.85 and from 0.64 to 0.76. In addition, the R^2 for the stems (Figure 3E) and laminae (Figure 3F) of SGHN and ZZN8 ranged from 0.71 to 0.75 and from 0.68 to 0.75, respectively. As a consequence, the fitting had good accuracy and was thus reliable. Further evaluation and analysis of the regression models for different organs showed that the best modeled color indices varied among different organs, and the high R^2 values (up to 0.94) indicated that the established predictive model had a good fit. Thus, it was feasible to establish a model for the anthocyanin content of purple corn plants by relating the anthocyanin content with the color parameters of visible light images of the purple corn plants.

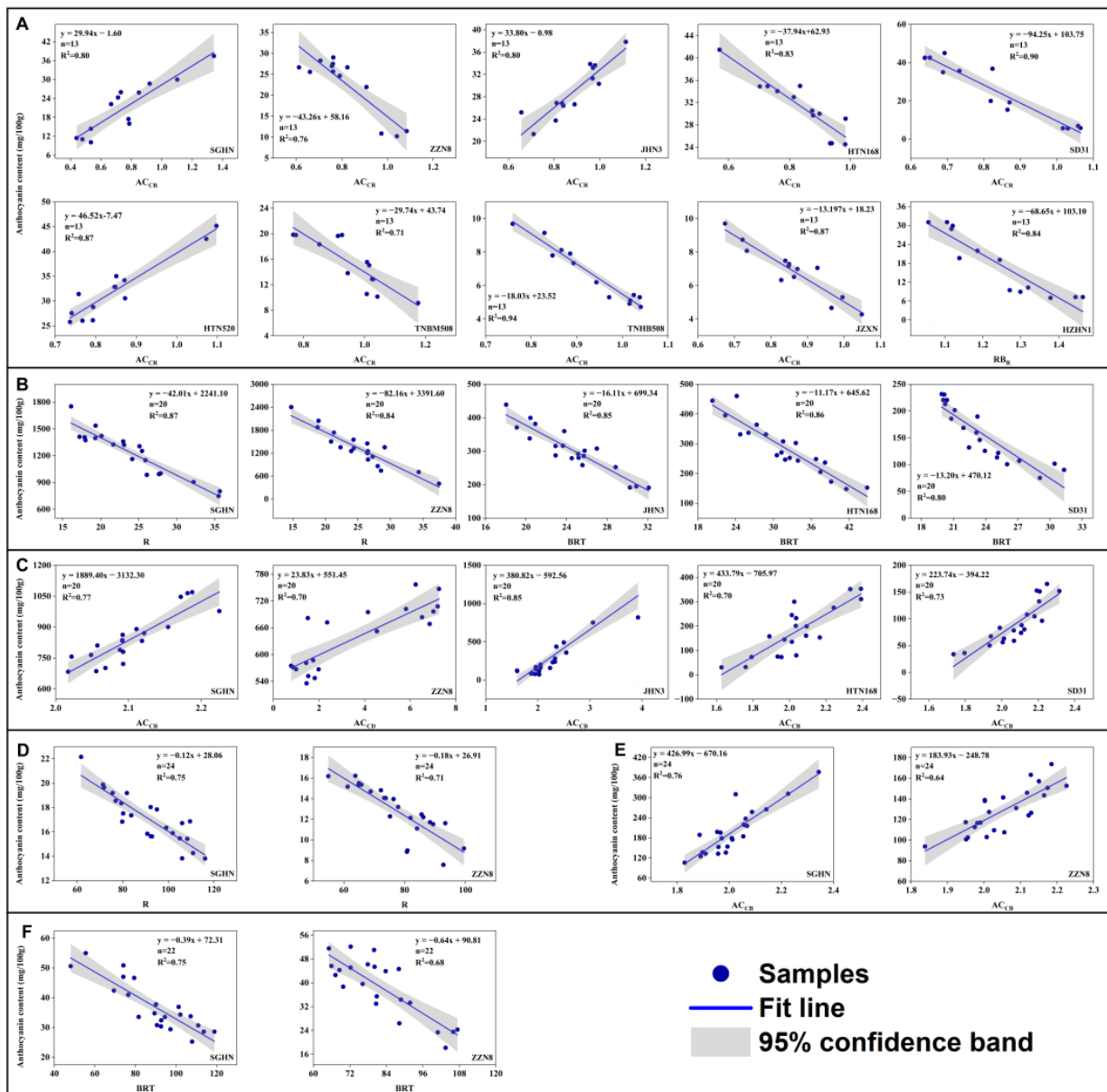


Figure 3. Fitting the relationship between anthocyanin content and the color index. The letters in the figure indicate grains (A); cobs (B); husks (C); stems (D); sheaths (E) and laminae (F).

Table 4. Coefficient of determination (R^2) and statistical significance of the fitting between anthocyanin content and color index.

Indices		R	G	B	RG _R	RB _R	GB _R	S _{red}	S _{green}	S _{blue}	C	BRT	AC _{CB}	AC _{CR}	AC _{CD}
SGHN	Grain	0.10	0.27 *	0.09	0.70 **	0.52 **	0.30 *	0.71 **	0.80 **	0.45 **	0.76 **	<0.01	0.77 **	0.80 **	0.76 **
	Cob	0.87 **	0.66 **	0.76 **	0.42 **	0.49 **	<0.01	0.47 **	0.34 **	0.42 **	0.43 **	0.82 **	0.34	0.34	0.73 **
	Husk	0.05	0.15	0.10	0.57 **	0.18	0.30	0.38 *	0.76 **	<0.01	0.56 **	0.10	0.77 **	0.76 **	0.61 **
	Stem	0.75 **	0.54 *	0.71 **	0.01	0.24	0.02	0.26	<0.01	0.15	0.02	0.71 **	<0.01	<0.01	<0.01
	Sheath	0.14	<0.01	0.25	0.51 **	<0.01	0.58 **	0.10	0.75 **	0.19	0.48 **	0.10	0.76 **	0.75 **	0.73 **
	Lamina	0.71 **	0.75 **	0.72 **	0.28	0.47 *	0.16	0.62 **	<0.01	0.31 *	0.27	0.75 **	<0.01	<0.01	<0.01
ZZN8	Grain	0.43 **	0.72 **	0.54 **	0.55 **	0.18	0.64 **	0.51 **	0.73 **	<0.01	0.64 **	0.55 **	0.63 **	0.76 **	0.52 **
	Cob	0.84 **	0.67 **	0.70 **	<0.01	<0.01	<0.01	<0.01	<0.01	<0.01	<0.01	0.79 **	<0.01	<0.01	0.17
	Husk	<0.01	0.10	0.03	0.61 **	0.36 **	0.34 **	0.51 **	0.67 **	0.08	0.60 **	0.00	0.67 **	0.67 **	0.70 **
	Stem	0.70 **	0.64 **	0.54 **	<0.01	0.18	0.32 *	<0.01	0.11	0.40 *	<0.01	0.67 **	0.11	0.11	0.03
	Sheath	0.02	0.05	<0.01	0.02	0.22 *	0.48 **	0.06	0.63 **	0.33 **	0.01	0.00	0.64 **	0.62 **	0.55 **
	Lamina	0.64 **	0.67 **	0.57 **	0.19	0.03	<0.01	0.21	<0.01	<0.01	0.19	0.68 **	<0.01	<0.01	0.12
JHN3	Grain	0.09	<0.01	<0.01	0.22	0.12	0.05	0.12	0.79 **	0.21	0.40 *	<0.01	0.16	0.79 **	0.65 **
	Cob	0.84 **	0.69 **	0.47 **	<0.01	<0.01	<0.01	<0.01	<0.01	<0.01	<0.01	0.85 **	<0.01	<0.01	0.23
	Husk	0.77 **	0.81 **	0.68 **	0.80 **	0.81 **	0.72 **	0.07	0.79 **	0.84 **	0.67 **	0.78 **	0.85 **	0.73 **	0.32 *
HTN168	Grain	0.02	0.36 *	<0.01	0.42 **	0.12	0.82 **	<0.01	0.82 **	0.37 *	0.26	0.06	0.79 **	0.83 **	0.58 **
	Cob	0.86 **	0.85 **	0.84 **	0.35 **	0.10	0.12	0.29 *	0.32 *	<0.01	0.35 **	0.86 **	0.32 *	0.31 *	0.30 *
	Husk	0.51 **	0.57 **	0.25 *	0.37 *	0.34 *	0.70 **	<0.01	0.67 **	0.57 **	0.34 *	0.49 **	0.70 **	0.66 **	0.60 **
SD31	Grain	0.55 **	0.58 **	0.54 **	0.87 **	0.57 **	0.48 **	0.80 **	0.90 **	0.14	0.87 **	0.56 **	0.89 **	0.90 **	0.55 **
	Cob	0.80 **	0.75 **	0.76 **	<0.01	0.04	<0.01	<0.01	<0.01	0.08	<0.01	0.80 **	<0.01	<0.01	0.30 *
	Husk	0.20	0.29 *	<0.01	0.23 *	0.51 **	0.73 **	0.10	0.70 **	0.66 **	0.20 *	0.13	0.73 **	0.69 **	0.58 **
HTN520	Grain	0.14	<0.01	<0.01	0.88 **	0.71 **	<0.01	0.85 **	0.88 **	0.60 **	0.70 **	<0.01	0.86 **	0.88 **	0.76 **
TNBM508	Grain	0.01	0.35 **	0.02	0.56 **	<0.01	0.70 **	0.34 **	0.70 **	0.34 **	0.58 **	0.11	0.67 **	0.71 **	0.60 **
TNHB509	Grain	0.65 **	0.71 **	0.56 **	0.69 **	0.08	0.46 **	0.38 **	0.94 **	<0.01	0.68 **	0.65 **	0.94 **	0.94 **	0.90 **
JZXN	Grain	0.40 **	0.64 **	0.55 **	0.86 **	0.71 **	0.42 **	0.84 **	0.86 **	0.33 **	0.87 **	0.53 **	0.87 **	0.86 **	0.54 **
HZHN1	Grain	<0.01	<0.01	<0.01	0.15	0.84 **	0.22	0.77 **	<0.01	0.61 **	0.18	<0.01	<0.01	<0.01	<0.01

Note: The highest R^2 for each species–tissue combination is highlighted in bold. Evaluation using Pearson’s correlation coefficients; * $p < 0.05$; ** $p < 0.01$.

3.4. Model Validation with an Independent Dataset

The predicted and measured values for different organs from all the varieties are presented (Figure 4). As a matter of fact, the samples were usually close to the 1:1 line. The RMSE values from the statistical results for model validation are shown in Table 5. The root mean square error (RMSE) was 0.31–6.85 mg/100 g in the grains, 16.55–36.59 mg/100 g in the cobs, 16.08–29.99 mg/100 g in the husks, 10.98–14.96 mg/100 g in the sheaths, 3.33–4.11 mg/100 g in the stems and 6.18–6.46 mg/100 g in the laminae. Meanwhile, the mean NRMSE values for the different organs were 11.68% for the grains, 13.66% for the cobs, 8.90% for the husks, 27.20% for the stems, 7.90% for the sheaths and 15.83% for the laminae. According to the model evaluation criteria mentioned above, it is not difficult to see that the predictive model has excellent accuracy and stability for the sheath and husk parts and also performs well for prediction of the anthocyanin content in the grains, cobs and laminae, but in the stem part, the NRMSE is between 20 and 30%, and the performance is not good.

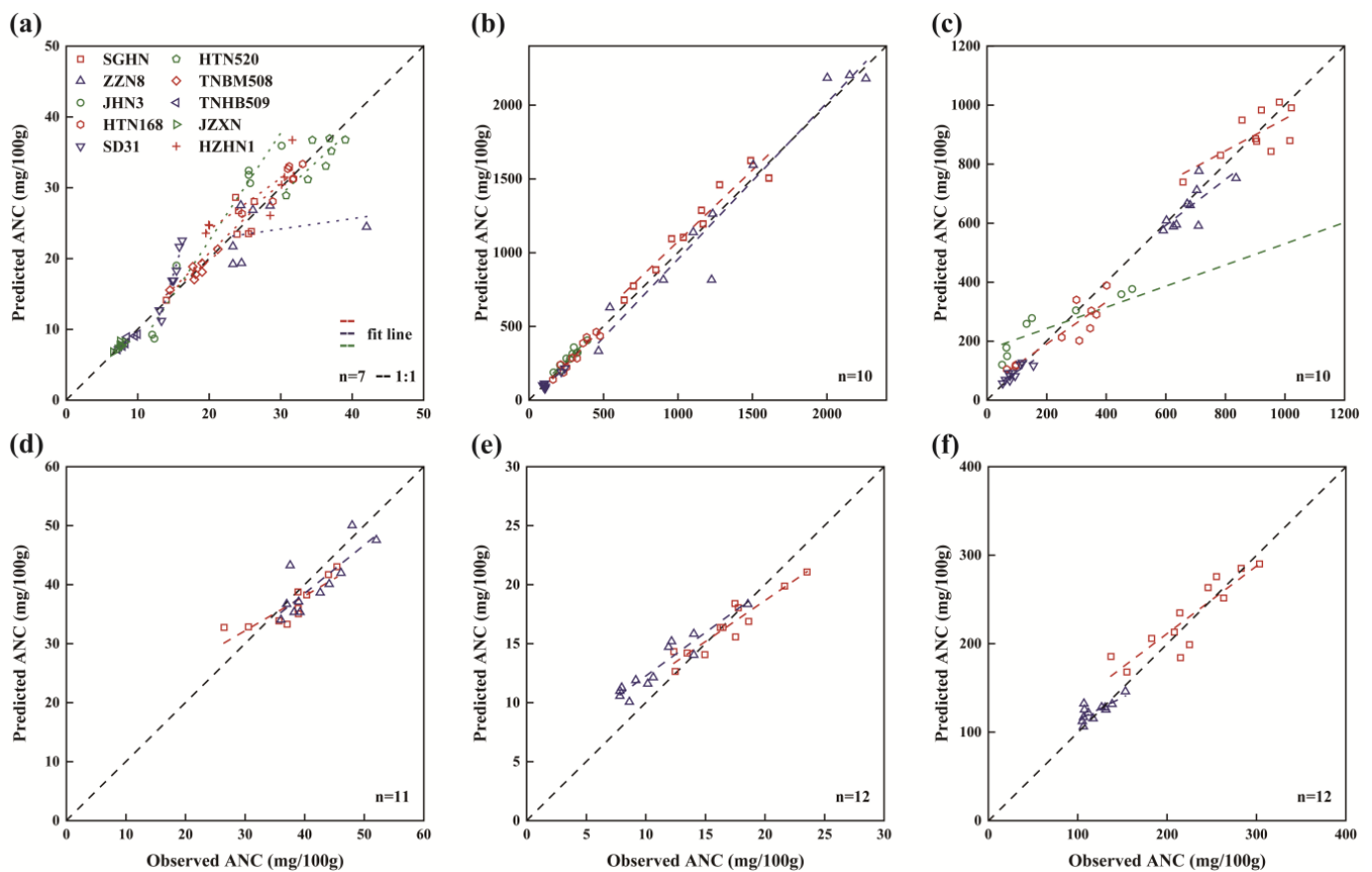


Figure 4. Validation of predictive models for anthocyanin content in different organs of purple corn; (a–f) are tests of anthocyanin content prediction models for grains, cobs, husks, laminae, stems and sheaths, respectively.

Table 5. Validation of predictive model for anthocyanin content based on color index.

Variety	Organ	Color Index	Validation	
			NRMSE (%)	RMSE (mg/100 g)
SGHN	Grain	AC _{CR}	15.05	3.51
ZZN8	Grain	AC _{CR}	16.19	4.44
JHN3	Grain	AC _{CR}	27.49	5.75

Table 5. Cont.

Variety	Organ	Color Index	Validation	
			NRMSE (%)	RMSE (mg/100 g)
HTN168	Grain	AC _{CR}	4.01	1.22
SD31	Grain	AC _{CR}	20.65	6.85
HTN520	Grain	AC _{CR}	6.35	2.25
TNBM508	Grain	AC _{CR}	4.25	0.77
TNHB509	Grain	AC _{CR}	5.04	0.42
JZXN	Grain	AC _{CB}	4.14	0.31
HZHN1	Grain	RB _R	13.60	3.50
SGHN	Cob	R	3.03	33.00
ZZN8	Cob	R	2.73	36.59
JHN3	Cob	BRT	6.04	16.55
HTN168	Cob	BRT	5.64	17.73
SD31	Cob	BRT	23.55	18.68
SGHN	Husk	AC _{CB}	3.33	29.99
ZZN8	Husk	AC _{CD}	3.84	26.02
JHN3	Husk	AC _{CB}	4.48	22.31
HTN168	Husk	AC _{CB}	6.22	16.08
SD31	Husk	AC _{CB}	26.62	24.13
SGHN	Stalk	R	24.35	4.11
ZZN8	Stalk	R	30.06	3.33
SGHN	Sheath	AC _{CB}	6.68	14.96
ZZN8	Sheath	AC _{CB}	9.11	10.98
SGHN	Lamina	BRT	16.18	6.18
ZZN8	Lamina	BRT	15.48	6.46

4. Discussion

4.1. Anthocyanins for Industry Use

Anthocyanins are widely used in cosmetics and in food colorings in industry [60–63]. Numerous studies have shown that anthocyanins have very good medicinal value and significant health effects, such as anti-cancer, anti-inflammation, anti-aging, anti-obesity and protection of vision [64–68]. A considerable supply of anthocyanins is required for industry use. To date, anthocyanins have primarily been sourced from by-products including the pomace and retentate of dark fruits and vegetables, such as black grapes, blueberries and purple carrots [15,69–71]. Obtaining anthocyanins using this strategy is relatively dear due to the high price of the raw materials, as well as the high costs of processing their residues. In addition, the anthocyanins obtained this way are very limited, as the material is left over after its primary use [15,18]. We found that the hybrids SGHN and ZZN8 had a high anthocyanin content. This provided a rich supply of anthocyanins. In particular, we also identified that the anthocyanin content of the cobs and husks was much higher than that of the other types of organs (Table 3), providing specific target organs for anthocyanin extraction [19,20,72]. Notably, purple corn is increasingly consumed as a fresh vegetable in Asian countries because of the health-promoting properties of the anthocyanin pigments in its aleurone or pericarp [73–76], which means that by-products such as its cobs and husk can be used as premium industrial raw materials for anthocyanin extraction. It can also maximize the economic value of the purple corn industry by utilizing by-product resources.

4.2. Modeling Robustness

AC_{CR} was shown to be the best index for nine varieties of grains but not for HZHN1. This unique abnormality could be due to the presence of white wax on the peel, thus causing obscure images [30,77,78]. It has also been reported that other factors such as the cell shape, cell wall thickness or pigment location may also alter the color perceived by sensors [79], causing errors whilst estimating the anthocyanin content from digital images. It is worth noting that using AC_{CB} for the husks of ZZN8 was not the best but it was still

chosen since there was only a minor difference in the fitting effect between AC_{CD} ($R^2 = 0.70$) and AC_{CB} ($R^2 = 0.68$). Hence, a unique color index that is suitable for a single organ was proposed. A similar situation existed for the predictive model for the cob sections. As such, the indices AC_{CR} , BRT, AC_{CB} , R, AC_{CB} and BRT were recommended for the grains, cobs, husks, stems, sheaths and laminae, respectively. The possible reason for this difference is that the anthocyanin content of different organ types varies greatly, which makes various organ surfaces show inconsistent colors. Despite the fact that digital photography may also fail when the cells of the measured surface are irregular, because visible light images can only capture two-dimensional planes of data [72,80,81]. But it is worth recognizing that numerical images showed better predictive performance than spectral reflectance images [28,82]. For example, digital images with spectrophotometer data were compared to analyze the petal colors of eight species with variable pigmentation patterns [83], which found that spectrophotometers may underestimate the variability in spectral signals when the patterns are complex. This is because the spectrometer probe holder has a relatively small sampling area, which may result in different spectral measurements depending on whether it is incidentally oriented toward light or dark stripes or patches [83]. Though this can be resolved by measuring the reflectance at multiple points, the time required for analysis will undoubtedly add up. Overall, it is undeniable that our proposed method for quantifying the content of anthocyanins in purple corn based on digital image representation has been proven to offer new opportunities to accurately quantify the concentration of anthocyanins in different organs of purple corn [1,84,85]. The main advantages of this method are its high efficiency and that it is completely non-invasive and applicable to plant samples of any size and shape.

4.3. Model Application

Purple corn is regarded as having the darkest grains in the plant kingdom. Anthocyanin is a multifunctional active substance in purple corn, which has potential health-promoting properties [86–88]. It has been widely promoted as a health food and has also attracted the attention of the food and drug industries [56,77,89]. The speed of obtaining a new variety using traditional breeding methods is limited by the acquisition of crop phenotypic data, particularly on tissue inclusions, so it is imperative to develop a high-throughput plant phenotyping analysis. Non-destructive data collected via ground-based and aerial HTP techniques are highly desirable for application in plant breeding since they can be used to assess different traits in large-scale field trials [90–92]. RGB cameras produce digital images, can mimic human visual perception and are available at a low price and a high resolution on the market, and image analysis using free software is simple and easy to learn and requires little training. Therefore, the RGB imaging approach represents a valuable and practical tool for breeders [93,94]. By applying predictive models, breeders and researchers can assess the anthocyanin content of a large number of purple corn varieties more quickly. This method can save time and costs and improve breeding efficiency in the development of more nutritious and commercially valuable varieties of purple corn. Therefore, after the appropriate adjustments, such as obtaining data from multiple locations and years, the model proposed in our study can be extended to ground and UAV platforms, expanding the monitoring range [95–98]. Nowadays, RGB imaging obtained with the rapid development of smartphones has led to the creation of applications with ever-increasing utility, such as the plant phenotyping apps Canopeo (v2.0) [99], Plant Screen Mobile (v1.6) [100] and PhenoApp (v1.0) [101]. As technological innovation advances, a real-time and rapid anthocyanin content estimation platform may be developed. As a consequence, the non-destructive, rapid, high-throughput evaluation of anthocyanin will have good potential to be applied to breeding or cultivation in the anthocyanin industry.

5. Conclusions

Purple corn has potential applications in industry due to its rich anthocyanin content. The anthocyanin content largely varied by organ type. This dissection of plants into specific organs identified the cobs of purple corn as a vital source providing anthocyanins for industry use. Digital image technology based on a RGB camera represents a rapid, non-destructive way to estimate plant tissue inclusions. A linear relationship between the anthocyanin content and the color indices derived from the RGB images was found for various types of organs, which was further used to establish a model for the prediction of the anthocyanin content. The model was then testified to have achieved good accuracy with its NRMSE in the range of 7.90–27.20%. However, considering the power and ability of deep learning, in future work, we will obtain more data through continuous observation to explore the application of deep learning to estimating the anthocyanin content in purple corn. Overall, this study provides a cheap imaging method for rapid assays of anthocyanin content.

Supplementary Materials: The following supporting information can be downloaded at: <https://www.mdpi.com/article/10.3390/agriculture14050744/s1>, Figure S1: Meteorological data of purple corn planting season (6.12 to 9.09) from 2021 to 2023; Table S1: Meteorological parameters of purple corn growth period from 2021 to 2023.

Author Contributions: Y.S. conceived of and supervised the study. Z.W. carried out the experiment and drafted the paper. Y.L., K.W. and C.X. contributed to drafting and the data analyses. Y.W., X.W. and J.L. helped with the sampling and data analyses. Y.S. and Y.L. improved the manuscript. All authors have read and agreed to the published version of the manuscript.

Funding: The work was supported by Anhui Province Natural Science Foundation (2208085MC59), and Provincial Grant No. 2021H254.

Institutional Review Board Statement: Not applicable.

Informed Consent Statement: Not applicable.

Data Availability Statement: The data presented in this study are available on request from the corresponding author.

Conflicts of Interest: The authors declare no conflicts of interest.

References

1. Custodio-Mendoza, J.A.; Aktaş, H.; Zalewska, M.; Wyrwisz, J.; Kurek, M.A. A Review of Quantitative and Topical Analysis of Anthocyanins in Food. *Molecules* **2024**, *29*, 1735. [[CrossRef](#)] [[PubMed](#)]
2. Cheaib, A.; Mahmoud, L.M.; Vincent, C.; Killiny, N.; Dutt, M. Influence of Anthocyanin Expression on the Performance of Photosynthesis in Sweet Orange, *Citrus sinensis* (L.) Osbeck. *Plants* **2023**, *12*, 3965. [[CrossRef](#)] [[PubMed](#)]
3. Landi, M.; Tattini, M.; Gould, K.S. Multiple functional roles of anthocyanins in plant-environment interactions. *Environ. Exp. Bot.* **2015**, *119*, 4–17. [[CrossRef](#)]
4. Marone, D.; Mastrangelo, A.M.; Borrelli, G.M.; Mores, A.; Laidò, G.; Russo, M.A.; Ficco, D.B.M. Specialized metabolites: Physiological and biochemical role in stress resistance, strategies to improve their accumulation, and new applications in crop breeding and management. *Plant Physiol. Biochem.* **2022**, *172*, 48–55. [[CrossRef](#)] [[PubMed](#)]
5. Liu, H.; Liu, Z.; Wu, Y.; Zheng, L.; Zhang, G. Regulatory Mechanisms of Anthocyanin Biosynthesis in Apple and Pear. *Int. J. Mol. Sci.* **2021**, *22*, 8441. [[CrossRef](#)] [[PubMed](#)]
6. Ma, Y.; Xiang, S.; Cui, Z.; Li, K.; Zhang, Z. Molecular Dynamic Regulation of Na and Mg Ions on Lithium Carbonate Crystallisation in Salt Lakes. *J. Wuhan Univ. Technol.-Mat. Sci. Edit.* **2021**, *36*, 22–28. [[CrossRef](#)]
7. Marino, M.; Gardana, C.; Rendine, M.; Klimis-Zacas, D.; Riso, P.; Porrini, M.; Del Bo', C. Nutritional and Phytochemical Characterization of Freeze-Dried Raspberry (*Rubus idaeus*): A Comprehensive Analysis. *Foods* **2024**, *13*, 1051. [[CrossRef](#)]
8. Cozzolino, D. Phenolics and spectroscopy: Challenges and successful stories in the grape and wine industry. *J. Sci. Food Agric.* **2023**. [[CrossRef](#)]
9. Chachar, Z.; Lai, R.; Ahmed, N.; Lingling, M.; Chachar, S.; Paker, N.P.; Qi, Y. Cloned genes and genetic regulation of anthocyanin biosynthesis in maize, a comparative review. *Front. Plant Sci.* **2024**, *15*, 1310634. [[CrossRef](#)]
10. García-Villegas, A.; Fernández-Ochoa, Á.; Alañón, M.E.; Rojas-García, A.; Arráez-Román, D.; Cádiz-Gurrea, M.d.I.L.; Segura-Carretero, A. Bioactive Compounds and Potential Health Benefits through Cosmetic Applications of Cherry Stem Extract. *Int. J. Mol. Sci.* **2024**, *25*, 3723. [[CrossRef](#)]

11. Global Flavonoids Market Size & Share Report, 2025. Available online: <https://www.grandviewresearch.com/industry-analysis/flavonoids-market> (accessed on 13 November 2023).
12. Romani, A.; Campo, M.; Urciuoli, S.; Marrone, G.; Noce, A.; Bernini, R. An Industrial and Sustainable Platform for the Production of Bioactive Micronized Powders and Extracts Enriched in Polyphenols from *Olea europaea* L. and *Vitis vinifera* L. Wastes. *Front. Nutr.* **2020**, *7*, 120. [[CrossRef](#)]
13. Leonarski, E.; Kuasnei, M.; Cesca, K.; de Oliveira, D.; Zielinski, A.A.F. Black rice and its by-products: Anthocyanin-rich extracts and their biological potential. *Crit. Rev. Food Sci. Nutr.* **2023**, 1–19. [[CrossRef](#)]
14. Silva, S.; Costa, E.M.; Calhau, C.; Morais, R.M.; Pintado, M.E. Anthocyanin extraction from plant tissues: A review. *Crit. Rev. Food Sci. Nutr.* **2017**, *57*, 3072–3083. [[CrossRef](#)]
15. Somavat, P.; Kumar, D.; Singh, V. Techno-economic feasibility analysis of blue and purple corn processing for anthocyanin extraction and ethanol production using modified dry grind process. *Ind. Crops Prod.* **2018**, *115*, 78–87. [[CrossRef](#)]
16. Jasińska, K.; Fabiszewska, A.; Białecka-Florjańczyk, E.; Zieniuk, B. Mini-Review on the Enzymatic Lipophilization of Phenolics Present in Plant Extracts with the Special Emphasis on Anthocyanins. *Antioxidants* **2022**, *11*, 1528. [[CrossRef](#)] [[PubMed](#)]
17. Carrillo, C.; Nieto, G.; Martínez-Zamora, L.; Ros, G.; Kamiloglu, S.; Munekata, P.E.S.; Pateiro, M.; Lorenzo, J.M.; Fernández-López, J.; Viuda-Martos, M.; et al. Novel Approaches for the Recovery of Natural Pigments with Potential Health Effects. *J. Agric. Food Chem.* **2022**, *70*, 6864–6883. [[CrossRef](#)]
18. Veloso, M.I.; Coelho, E.; Trabulo, O.; Coimbra, M.A. Elderberry Concentrate Juice Industrial By-Products Characterization and Valorisation. *Appl. Sci.* **2022**, *12*, 9463. [[CrossRef](#)]
19. Li, C.-Y.; Kim, H.-W.; Won, S.; Min, H.-K.; Park, K.-J.; Park, J.-Y.; Ahn, M.-S.; Rhee, H.-I. Corn Husk as a Potential Source of Anthocyanins. *J. Agric. Food Chem.* **2008**, *56*, 11413–11416. [[CrossRef](#)] [[PubMed](#)]
20. Fernandez-Aulis, F.; Hernandez-Vazquez, L.; Aguilar-Osorio, G.; Arrieta-Baez, D.; Navarro-Ocana, A. Extraction and Identification of Anthocyanins in Corn Cob and Corn Husk from Cacahuacintle Maize. *J. Food Sci.* **2019**, *84*, 954–962. [[CrossRef](#)]
21. Hong, H.T.; Netzel, M.E.; O'Hare, T.J. Optimisation of extraction procedure and development of LC–DAD–MS methodology for anthocyanin analysis in anthocyanin-pigmented corn kernels. *Food Chem.* **2020**, *319*, 126515. [[CrossRef](#)]
22. Ata-Ul-Karim, S.T.; Cao, Q.; Zhu, Y.; Tang, L.; Rehmani, M.I.A.; Cao, W. Non-destructive Assessment of Plant Nitrogen Parameters Using Leaf Chlorophyll Measurements in Rice. *Front. Plant Sci.* **2016**, *7*, 1829. [[CrossRef](#)] [[PubMed](#)]
23. Ji, Y.; Chen, Z.; Cheng, Q.; Liu, R.; Li, M.; Yan, X.; Li, G.; Wang, D.; Fu, L.; Ma, Y.; et al. Estimation of plant height and yield based on UAV imagery in faba bean (*Vicia faba* L.). *Plant Methods* **2022**, *18*, 26. [[CrossRef](#)] [[PubMed](#)]
24. Huang, H.; Deng, J.; Lan, Y.; Yang, A.; Zhang, L.; Wen, S.; Zhang, H.; Zhang, Y.; Deng, Y. Detection of Helminthosporium Leaf Blotch Disease Based on UAV Imagery. *Appl. Sci.* **2019**, *9*, 558. [[CrossRef](#)]
25. Heidarian Dehkordi, R.; El Jarroudi, M.; Kouadio, L.; Meersmans, J.; Beyer, M. Monitoring Wheat Leaf Rust and Stripe Rust in Winter Wheat Using High-Resolution UAV-Based Red-Green-Blue Imagery. *Remote Sens.* **2020**, *12*, 3696. [[CrossRef](#)]
26. Wan, L.; Zhang, J.; Dong, X.; Du, X.; Cen, H. Unmanned aerial vehicle-based field phenotyping of crop biomass using growth traits retrieved from PROSAIL model. *Comput. Electron. Agric.* **2021**, *187*, 106304. [[CrossRef](#)]
27. Makanza, R.; Zaman-Allah, M.; Cairns, J.E.; Magorokosho, C.; Tarekgegne, A.; Olsen, M.; Prasanna, B.M. High-Throughput Phenotyping of Canopy Cover and Senescence in Maize Field Trials Using Aerial Digital Canopy Imaging. *Remote Sens.* **2018**, *10*, 330. [[CrossRef](#)] [[PubMed](#)]
28. del Valle, J.C.; Gallardo-López, A.; Buide, M.L.; Whittall, J.B.; Narbona, E. Digital photography provides a fast, reliable, and noninvasive method to estimate anthocyanin pigment concentration in reproductive and vegetative plant tissues. *Ecol. Evol.* **2018**, *8*, 3064–3076. [[CrossRef](#)] [[PubMed](#)]
29. Gong, L.; Zhu, C.; Luo, Y.; Fu, X. Spectral Reflectance Reconstruction from Red-Green-Blue (RGB) Images for Chlorophyll Content Detection. *Appl. Spectrosc.* **2023**, *77*, 200–209. [[CrossRef](#)] [[PubMed](#)]
30. Riccardi, M.; Mele, G.; Pulvento, C.; Lavini, A.; d'Andria, R.; Jacobsen, S.-E. Non-destructive evaluation of chlorophyll content in quinoa and amaranth leaves by simple and multiple regression analysis of RGB image components. *Photosynth. Res.* **2014**, *120*, 263–272. [[CrossRef](#)]
31. Wood, N.J.; Baker, A.; Quinnell, R.J.; Camargo-Valero, M.A. A Simple and Non-destructive Method for Chlorophyll Quantification of Chlamydomonas Cultures Using Digital Image Analysis. *Front. Bioeng. Biotechnol.* **2020**, *8*, 746. [[CrossRef](#)]
32. Wang, Y.; Wang, D.; Shi, P.; Omasa, K. Estimating rice chlorophyll content and leaf nitrogen concentration with a digital still color camera under natural light. *Plant Methods* **2014**, *10*, 36. [[CrossRef](#)] [[PubMed](#)]
33. Faragó, D.; Sass, L.; Valkai, I.; András, N.; Szabados, L. PlantSize Offers an Affordable, Non-destructive Method to Measure Plant Size and Color in Vitro. *Front. Plant Sci.* **2018**, *9*, 219. [[CrossRef](#)] [[PubMed](#)]
34. Zhang, H.; Ge, Y.; Xie, X.; Atefi, A.; Wijewardane, N.K.; Thapa, S. High throughput analysis of leaf chlorophyll content in sorghum using RGB, hyperspectral, and fluorescence imaging and sensor fusion. *Plant Methods* **2022**, *18*, 60. [[CrossRef](#)] [[PubMed](#)]
35. Bennett, C.; Sookwong, P.; Jakmunee, J.; Mahatheeranont, S. Smartphone digital image colorimetric determination of the total monomeric anthocyanin content in black rice via the pH differential method. *Anal. Methods* **2021**, *13*, 3348–3358. [[CrossRef](#)] [[PubMed](#)]
36. Junker, L.V.; Ensminger, I. Relationship between leaf optical properties, chlorophyll fluorescence and pigment changes in senescing Acer saccharum leaves. *Tree Physiol.* **2016**, *36*, 694–711. [[CrossRef](#)]

37. Wang, Z.; Sun, W.; Liu, X.; Li, Y.; Collins, B.; Ullah, N.; Song, Y. Analysis on Heat Characteristics for Summer Maize Cropping in a Semi-Arid Region. *Agronomy* **2022**, *12*, 1435. [[CrossRef](#)]
38. Andersen, Ø.M.; Jordheim, M. Anthocyanins. In *Encyclopedia of Life Sciences*; John Wiley & Sons, Ltd.: Hoboken, NJ, USA, 2010; ISBN 978-0-470-01590-2.
39. Alappat, B.; Alappat, J. Anthocyanin Pigments: Beyond Aesthetics. *Molecules* **2020**, *25*, 5500. [[CrossRef](#)]
40. White, T.E.; Dalrymple, R.L.; Noble, D.W.A.; O'Hanlon, J.C.; Zurek, D.B.; Umbers, K.D.L. Reproducible research in the study of biological coloration. *Anim. Behav.* **2015**, *106*, 51–57. [[CrossRef](#)]
41. Stevens, M.; Párraga, C.A.; Cuthill, I.C.; Partridge, J.C.; Troscianko, T.S. Using digital photography to study animal coloration. *Biol. J. Linn. Soc.* **2007**, *90*, 211–237. [[CrossRef](#)]
42. Akkaynak, D.; Treibitz, T.; Xiao, B.; Gürkan, U.A.; Allen, J.J.; Demirci, U.; Hanlon, R.T. Use of commercial off-the-shelf digital cameras for scientific data acquisition and scene-specific color calibration. *J. Opt. Soc. Am. A JOSAA* **2014**, *31*, 312–321. [[CrossRef](#)]
43. Tedla, S.; Wang, Y.; Patel, M.; Brown, M.S. Analyzing color imaging failure on consumer-grade cameras. *J. Opt. Soc. Am. A JOSAA* **2022**, *39*, B21–B27. [[CrossRef](#)] [[PubMed](#)]
44. Liang, Y.; Urano, D.; Liao, K.-L.; Hedrick, T.L.; Gao, Y.; Jones, A.M. A nondestructive method to estimate the chlorophyll content of Arabidopsis seedlings. *Plant Methods* **2017**, *13*, 26. [[CrossRef](#)] [[PubMed](#)]
45. Mathieu, R.; Pouget, M.; Cervelle, B.; Escadafal, R. Relationships between Satellite-Based Radiometric Indices Simulated Using Laboratory Reflectance Data and Typic Soil Color of an Arid Environment. *Remote Sens. Environ.* **1998**, *66*, 17–28. [[CrossRef](#)]
46. Mizunuma, T.; Mencuccini, M.; Wingate, L.; Ogee, J.; Nichol, C.; Grace, J. Sensitivity of colour indices for discriminating leaf colours from digital photographs. *Methods Ecol. Evol.* **2014**, *5*, 1078–1085. [[CrossRef](#)]
47. Tan, J.; Han, Y.; Han, B.; Qi, X.; Cai, X.; Ge, S.; Xue, H. Extraction and purification of anthocyanins: A review. *J. Agric. Food Res.* **2022**, *8*, 100306. [[CrossRef](#)]
48. Bai, X.; Zhou, L.; Zhou, L.; Cang, S.; Liu, Y.; Liu, R.; Liu, J.; Feng, X.; Fan, R. The Research Progress of Extraction, Purification and Analysis Methods of Phenolic Compounds from Blueberry: A Comprehensive Review. *Molecules* **2023**, *28*, 3610. [[CrossRef](#)]
49. Warton, D.I.; Wright, I.J.; Falster, D.S.; Westoby, M. Bivariate line-fitting methods for allometry. *Biol. Rev. Camb. Philos. Soc.* **2006**, *81*, 259–291. [[CrossRef](#)]
50. Zhang, P.; Wang, X.; Song, P.X.K.; Zhang, J.Y.; So, W.F.K.; Team, T.M.S.; Sugar, C.A.; James, G.M.; Serban, N.; Wasserman, L. *The R Book*; John Wiley & Sons, Ltd.: Hoboken, NJ, USA, 2012; pp. 449–497, ISBN 978-1-118-44890-8.
51. Loague, K.; Green, R.E. Statistical and graphical methods for evaluating solute transport models: Overview and application. *J. Contam. Hydrol.* **1991**, *7*, 51–73. [[CrossRef](#)]
52. Qiao, L.; Tang, W.; Gao, D.; Zhao, R.; An, L.; Li, M.; Sun, H.; Song, D. UAV-based chlorophyll content estimation by evaluating vegetation index responses under different crop coverages. *Comput. Electron. Agric.* **2022**, *196*, 106775. [[CrossRef](#)]
53. Kim, C.; van Iersel, M.W. Image-based phenotyping to estimate anthocyanin concentrations in lettuce. *Front. Plant Sci.* **2023**, *14*, 1155722. [[CrossRef](#)]
54. He, L.; Sun, W.; Chen, X.; Han, L.; Li, J.; Ma, Y.; Song, Y. Modeling Maize Canopy Morphology in Response to Increased Plant Density. *Front. Plant Sci.* **2021**, *11*, 533514. [[CrossRef](#)] [[PubMed](#)]
55. Cuevas Montilla, E.; Hillebrand, S.; Antezana, A.; Winterhalter, P. Soluble and Bound Phenolic Compounds in Different Bolivian Purple Corn (*Zea mays* L.) Cultivars. *J. Agric. Food Chem.* **2011**, *59*, 7068–7074. [[CrossRef](#)] [[PubMed](#)]
56. Cai, T.; Ge-Zhang, S.; Song, M. Anthocyanins in metabolites of purple corn. *Front. Plant Sci.* **2023**, *14*, 1154535. [[CrossRef](#)] [[PubMed](#)]
57. Gullón, P.; Eibes, G.; Lorenzo, J.M.; Pérez-Rodríguez, N.; Lú-Chau, T.A.; Gullón, B. Green sustainable process to revalorize purple corn cobs within a biorefinery frame: Co-production of bioactive extracts. *Sci. Total Environ.* **2020**, *709*, 136236. [[CrossRef](#)] [[PubMed](#)]
58. Yadav, S.P.; Ibaraki, Y.; Gupta, S.D. Estimation of the chlorophyll content of micropropagated potato plants using RGB based image analysis. *Plant Cell Tissue Organ. Cult.* **2010**, *100*, 183–188. [[CrossRef](#)]
59. Lou, H.; Hu, Y.; Zhang, L.; Sun, P.; Lu, H. Nondestructive evaluation of the changes of total flavonoid, total phenols, ABTS and DPPH radical scavenging activities, and sugars during mulberry (*Morus alba* L.) fruits development by chlorophyll fluorescence and RGB intensity values. *LWT-Food Sci. Technol.* **2012**, *47*, 19–24. [[CrossRef](#)]
60. Qin, Y.; Liu, Y.; Yong, H.; Liu, J.; Zhang, X.; Liu, J. Preparation and characterization of active and intelligent packaging films based on cassava starch and anthocyanins from *Lycium ruthenicum* Murr. *Int. J. Biol. Macromol.* **2019**, *134*, 80–90. [[CrossRef](#)] [[PubMed](#)]
61. Ghareaghajlou, N.; Hallaj-Nezhadi, S.; Ghasempour, Z. Red cabbage anthocyanins: Stability, extraction, biological activities and applications in food systems. *Food Chem.* **2021**, *365*, 130482. [[CrossRef](#)]
62. Brudzyńska, P.; Sionkowska, A.; Grisel, M. Plant-Derived Colorants for Food, Cosmetic and Textile Industries: A Review. *Materials* **2021**, *14*, 3484. [[CrossRef](#)]
63. Cai, D.; Li, X.; Chen, J.; Jiang, X.; Ma, X.; Sun, J.; Tian, L.; Vidyarthi, S.K.; Xu, J.; Pan, Z.; et al. A comprehensive review on innovative and advanced stabilization approaches of anthocyanin by modifying structure and controlling environmental factors. *Food Chem.* **2022**, *366*, 130611. [[CrossRef](#)]
64. Calderón-Reyes, C.; Pezoa, R.S.; Leal, P.; Ribera-Fonseca, A.; Cáceres, C.; Riquelme, I.; Zambrano, T.; Peña, D.; Alberdi, M.; Reyes-Díaz, M. Anthocyanin-Rich Extracts of Calafate (*Berberis microphylla* G. Forst.) Fruits Decrease In Vitro Viability and Migration of Human Gastric and Gallbladder Cancer Cell Lines. *J. Soil. Sci. Plant Nutr.* **2020**, *20*, 1891–1903. [[CrossRef](#)]

65. Gašić, U.; Ćirić, I.; Pejić, T.; Radenković, D.; Djordjević, V.; Radulović, S.; Tešić, Ž. Polyphenols as Possible Agents for Pancreatic Diseases. *Antioxidants* **2020**, *9*, 547. [[CrossRef](#)] [[PubMed](#)]
66. Matboli, M.; Hasanin, A.H.; Hussein, R.; El-Nakeep, S.; Habib, E.K.; Ellackany, R.; Saleh, L.A. Cyanidin 3-glucoside modulated cell cycle progression in liver precancerous lesion, in vivo study. *World J. Gastroenterol.* **2021**, *27*, 1435–1450. [[CrossRef](#)] [[PubMed](#)]
67. Park, S.; Choi, M.; Lee, M. Effects of Anthocyanin Supplementation on Reduction of Obesity Criteria: A Systematic Review and Meta-Analysis of Randomized Controlled Trials. *Nutrients* **2021**, *13*, 2121. [[CrossRef](#)] [[PubMed](#)]
68. Tang, S.; Kan, J.; Sun, R.; Cai, H.; Hong, J.; Jin, C.; Zong, S. Anthocyanins from purple sweet potato alleviate doxorubicin-induced cardiotoxicity in vitro and in vivo. *J. Food Biochem.* **2021**, *45*, e13869. [[CrossRef](#)]
69. Bechtold, T.; Mahmud-Ali, A.; Mussak, R. Anthocyanin dyes extracted from grape pomace for the purpose of textile dyeing. *J. Sci. Food Agric.* **2007**, *87*, 2589–2595. [[CrossRef](#)] [[PubMed](#)]
70. Barnes, J.S.; Nguyen, H.P.; Shen, S.; Schug, K.A. General method for extraction of blueberry anthocyanins and identification using high performance liquid chromatography–electrospray ionization-ion trap-time of flight-mass spectrometry. *J. Chromatogr. A* **2009**, *1216*, 4728–4735. [[CrossRef](#)] [[PubMed](#)]
71. Assous, M.T.M.; Abdel-Hady, M.M.; Medany, G.M. Evaluation of red pigment extracted from purple carrots and its utilization as antioxidant and natural food colorants. *Ann. Agric. Sci.* **2014**, *59*, 1–7. [[CrossRef](#)]
72. Tanner, F.; Tonn, S.; de Wit, J.; Van den Ackerveken, G.; Berger, B.; Plett, D. Sensor-based phenotyping of above-ground plant-pathogen interactions. *Plant Methods* **2022**, *18*, 35. [[CrossRef](#)]
73. Choe, E.; Rocheford, T.R. Genetic and QTL analysis of pericarp thickness and ear architecture traits of Korean waxy corn germplasm. *Euphytica* **2012**, *183*, 243–260. [[CrossRef](#)]
74. Lim, S.; Yi, G. Investigating seed mineral composition in Korean landrace maize (*Zea mays* L.) and its kernel texture specificity. *J. Integr. Agric.* **2019**, *18*, 1996–2005. [[CrossRef](#)]
75. Salvador-Reyes, R.; Clerici, M.T.P.S. Peruvian Andean maize: General characteristics, nutritional properties, bioactive compounds, and culinary uses. *Food Res. Int.* **2020**, *130*, 108934. [[CrossRef](#)] [[PubMed](#)]
76. Kim, J.-T.; Yi, G.; Chung, I.-M.; Son, B.-Y.; Bae, H.-H.; Go, Y.S.; Ha, J.Y.; Baek, S.-B.; Kim, S.-L. Timing and Pattern of Anthocyanin Accumulation during Grain Filling in Purple Waxy Corn (*Zea mays* L.) Suggest Optimal Harvest Dates. *ACS Omega* **2020**, *5*, 15702–15708. [[CrossRef](#)] [[PubMed](#)]
77. Chatham, L.A.; Paulsmeyer, M.; Juvik, J.A. Prospects for economical natural colorants: Insights from maize. *Theor. Appl. Genet.* **2019**, *132*, 2927–2946. [[CrossRef](#)] [[PubMed](#)]
78. Menozzi, C.; Calvini, R.; Nigro, G.; Tessarin, P.; Bossio, D.; Calderisi, M.; Ferrari, V.; Foca, G.; Ulrici, A. Design and application of a smartphone-based device for in vineyard determination of anthocyanins content in red grapes. *Microchem. J.* **2023**, *191*, 108811. [[CrossRef](#)]
79. Ingrouille, M. Understanding flowers and flowering: An integrated approach. *Ann. Bot.* **2009**, *103*, vi–vii. [[CrossRef](#)]
80. Kay, Q.O.N.; Daoud, H.S.; Stirton, C.H. Pigment distribution, light reflection and cell structure in petals. *Bot. J. Linn. Soc.* **1981**, *83*, 57–83. [[CrossRef](#)]
81. van der Kooij, C.J.; Elzenga, J.T.M.; Staal, M.; Stavenga, D.G. How to colour a flower: On the optical principles of flower coloration. *Proc. Biol. Sci.* **2016**, *283*, 20160429. [[CrossRef](#)] [[PubMed](#)]
82. Gómez, J.; Lián-Cembrano, G. SpotEgg: An image-processing tool for automatized analysis of colouration and spottiness. *J. Avian Biol.* **2017**, *48*, 502–512. [[CrossRef](#)]
83. Garcia, J.E.; Greentree, A.D.; Shrestha, M.; Dorin, A.; Dyer, A.G. Flower colours through the lens: Quantitative measurement with visible and ultraviolet digital photography. *PLoS ONE* **2014**, *9*, e96646. [[CrossRef](#)]
84. Berger, K.; Machwitz, M.; Kycko, M.; Kefauver, S.C.; Van Wittenberghe, S.; Gerhards, M.; Verrelst, J.; Atzberger, C.; van der Tol, C.; Damm, A.; et al. Multi-sensor spectral synergies for crop stress detection and monitoring in the optical domain: A review. *Remote Sens. Environ.* **2022**, *280*, 113198. [[CrossRef](#)] [[PubMed](#)]
85. Liu, Y.; Zhang, Y.; Zhou, Y.; Feng, X. Anthocyanins in Different Food Matrices: Recent Updates on Extraction, Purification and Analysis Techniques. *Crit. Rev. Anal. Chem.* **2022**, 1–32. [[CrossRef](#)]
86. Petroni, K.; Pilu, R.; Tonelli, C. Anthocyanins in corn: A wealth of genes for human health. *Planta* **2014**, *240*, 901–911. [[CrossRef](#)]
87. Lao, F.; Sigurdson, G.T.; Giusti, M.M. Health Benefits of Purple Corn (*Zea mays* L.) Phenolic Compounds. *Compr. Rev. Food Sci. Food Saf.* **2017**, *16*, 234–246. [[CrossRef](#)] [[PubMed](#)]
88. Elisa, D.-H.; Marcela, G.-M.; Janet Alejandra, G.-U.; Martha Elena, D.-H. The nutraceutical value of maize (*Zea mays* L.) landraces and the determinants of its variability: A review. *J. Cereal Sci.* **2022**, *103*, 103399. [[CrossRef](#)]
89. Robles-Plata, V.T.; Serna Saldivar, S.; de Dios Figueroa-Cárdenas, J.; Rooney, W.L.; Dávila-Vega, J.P.; Chuck-Hernández, C.; Escalante-Aburto, A. Biophysical, Nutraceutical, and Technofunctional Features of Specialty Cereals: Pigmented Popcorn and Sorghum. *Foods* **2023**, *12*, 2301. [[CrossRef](#)]
90. Loladze, A.; Rodrigues, F.A.; Toledo, F.; San Vicente, F.; Gérard, B.; Boddupalli, M.P. Application of Remote Sensing for Phenotyping Tar Spot Complex Resistance in Maize. *Front. Plant Sci.* **2019**, *10*, 552. [[CrossRef](#)]
91. Watt, M.; Fiorani, F.; Usadel, B.; Rascher, U.; Muller, O.; Schurr, U. Phenotyping: New Windows into the Plant for Breeders. *Annu. Rev. Plant Biol.* **2020**, *71*, 689–712. [[CrossRef](#)]
92. Lobos, G.A.; Estrada, F.; Del Pozo, A.; Romero-Bravo, S.; Astudillo, C.A.; Mora-Poblete, F. Challenges for a Massive Implementation of Phenomics in Plant Breeding Programs. *Methods Mol. Biol.* **2022**, *2539*, 135–157. [[CrossRef](#)]

93. Hu, Y.; Schmidhalter, U. Opportunity and challenges of phenotyping plant salt tolerance. *Trends Plant Sci.* **2023**, *28*, 552–566. [[CrossRef](#)]
94. Rößle, D.; Prey, L.; Ramgraber, L.; Hanemann, A.; Cremers, D.; Noack, P.O.; Schön, T. Efficient Noninvasive FHB Estimation using RGB Images from a Novel Multiyear, Multirater Dataset. *Plant Phenomics* **2023**, *5*, 0068. [[CrossRef](#)] [[PubMed](#)]
95. Jiang, Z.; Tu, H.; Bai, B.; Yang, C.; Zhao, B.; Guo, Z.; Liu, Q.; Zhao, H.; Yang, W.; Xiong, L.; et al. Combining UAV-RGB high-throughput field phenotyping and genome-wide association study to reveal genetic variation of rice germplasms in dynamic response to drought stress. *New Phytol.* **2021**, *232*, 440–455. [[CrossRef](#)] [[PubMed](#)]
96. Shu, M.; Fei, S.; Zhang, B.; Yang, X.; Guo, Y.; Li, B.; Ma, Y. Application of UAV Multisensor Data and Ensemble Approach for High-Throughput Estimation of Maize Phenotyping Traits. *Plant Phenomics* **2022**, *2022*, 9802585. [[CrossRef](#)] [[PubMed](#)]
97. Fei, S.; Hassan, M.A.; Xiao, Y.; Su, X.; Chen, Z.; Cheng, Q.; Duan, F.; Chen, R.; Ma, Y. UAV-based multi-sensor data fusion and machine learning algorithm for yield prediction in wheat. *Precis. Agric.* **2023**, *24*, 187–212. [[CrossRef](#)] [[PubMed](#)]
98. Sarkar, S.; Zhou, J.; Scaboo, A.; Zhou, J.; Aloysius, N.; Lim, T.T. Assessment of Soybean Lodging Using UAV Imagery and Machine Learning. *Plants* **2023**, *12*, 2893. [[CrossRef](#)] [[PubMed](#)]
99. Patrignani, A.; Ochsner, T.E. Canopeo: A Powerful New Tool for Measuring Fractional Green Canopy Cover. *Agron. J.* **2015**, *107*, 2312–2320. [[CrossRef](#)]
100. Müller-Linow, M.; Wilhelm, J.; Briese, C.; Wojciechowski, T.; Schurr, U.; Fiorani, F. Plant Screen Mobile: An open-source mobile device app for plant trait analysis. *Plant Methods* **2019**, *15*, 2. [[CrossRef](#)]
101. Röckel, F.; Schreiber, T.; Schüler, D.; Braun, U.; Krukenberg, I.; Schwander, F.; Peil, A.; Brandt, C.; Willner, E.; Gransow, D.; et al. PhenoApp: A mobile tool for plant phenotyping to record field and greenhouse observations. *F1000Research* **2022**, *11*, 12. [[CrossRef](#)]

Disclaimer/Publisher’s Note: The statements, opinions and data contained in all publications are solely those of the individual author(s) and contributor(s) and not of MDPI and/or the editor(s). MDPI and/or the editor(s) disclaim responsibility for any injury to people or property resulting from any ideas, methods, instructions or products referred to in the content.